

Incommensurate phases of a bosonic two-leg ladder under a flux

E. Orignac

*Laboratoire de Physique de l'École Normale Supérieure de Lyon,
CNRS UMR5672, 46 Allée d'Italie, F-69364 Lyon Cedex 7, France*

R. Citro

*Dipartimento di Fisica "E.R. Caianiello", Università degli Studi di Salerno,
Via Ponte Don Melillo, I-84084 Fisciano (Sa), Italy*

M. Di Dio

CNR-IOM-Democritos National Simulation Centre, UDS Via Bonomea 265, I-34136, Trieste, Italy

S. De Palo

*CNR-IOM-Democritos National Simulation Centre,
UDS Via Bonomea 265, I-34136, Trieste, Italy and
Dipartimento di Fisica Teorica, Università Trieste, Trieste, Italy*

M.-L. Chiofalo

Dept. of Physics "Enrico Fermi" and INFN, Università di Pisa Largo Bruno Pontecorvo 3 I-56127 Pisa, Italy

(Dated: December 3, 2024)

A boson two-leg ladder in the presence of a synthetic magnetic flux is investigated by means of bosonization techniques and Density Matrix Renormalization Group (DMRG). We follow the quantum phase transition from commensurate Meissner to an incommensurate vortex phase with increasing flux spanning different fillings. When the applied flux is $\rho\pi$ and close to it, where ρ is the filling per rung, we predict and find the formation of a second type of incommensuration in the vortex state that could be detectable in physical observables, like the momentum distribution. We characterize this new phase by analyzing the rung-rung correlation function together with the static spin and charge correlation functions.

A remarkable characteristic of charged systems with broken $U(1)$ global gauge symmetry such as superconductors is the Meissner-Ochsenfeld effect¹. In the Meissner phase, below the critical field H_{c1} , a superconductor behaves as a perfect diamagnetic, i.e. it develops surface currents that fully screen the external magnetic field. In a type-II superconductor, for fields above $H > H_{c1}$, an Abrikosov vortex lattice phase is formed in the system, where the magnetic field partially penetrates into. In quasi one-dimensional systems, analogues of the Meissner and Abrikosov vortex lattice have been predicted for the bosonic two-leg ladder²⁻⁴, the simplest system where orbital magnetic field effects are allowed. It was shown that in this model, the quantum phase transition between the Meissner and the Vortex phase is a commensurate-incommensurate transition⁵⁻⁷. Chiral order in such models has been analyzed both analytically^{2,8} and numerically⁹ in the limit of half a flux quantum per plaquette. More recently, it was shown for ladder systems at commensurate filling that a chiral Mott insulator phase could be obtained¹⁰⁻¹³. Initially, Josephson junction arrays¹⁴⁻¹⁷ were proposed as experimental realizations of bosonic one dimensional systems.^{18,19} However, Josephson junctions are dissipative and open systems^{20,20-22} that cannot be described using a simple many-body Hamiltonian and the quantum effects in the vortex phase of the Josephson ladder are weak.²³ Fortunately, with the recent advent of ultracold atomic gases, another route to realize low dimensional strongly interacting bosonic systems has opened²⁴⁻²⁶. Atoms being neutral, it is necessary to find a way to realize an artificial magnetic flux acting on the ladder, e.g. using geometric phases, or the spin-orbit coupling. Indeed, there is a mapping of the two-leg ladder bosonic model to a two-component spinor boson model in which the bosons in the upper leg become spin-up bosons and the bosons in the lower leg spin-down bosons. Under such mapping, the magnetic flux of the ladder becomes a spin-orbit coupling for the spinor bosons. Theoretical proposals to realize either artificial gauge fields and artificial spin orbit coupling have been put forward^{27,28}, and recently an artificial spin-orbit coupling has been achieved in a cold atoms experiment²⁹. See³⁰ for a review. Thus, cold atom systems represent the prime candidates where to probe the Meissner effect through the realization of synthetic gauge fields. Indeed, recently, the Meissner effect and the formation of a vortex state have been observed for non-interacting bosons in flux ladders of ultracold atoms, with artificial gauge fields induced by laser-assisted tunneling³¹. The behavior of the chiral current as a function of the coupling strengths along the rungs of the ladder, indicates a diamagnetic phase when it reaches a saturated maximum and a vortex lattice phase when it starts to decrease. This experimental achievement has revived the theoretical interest for bosonic ladders in the presence of magnetic flux and its spinor-boson equivalent in the presence of interaction, where an even richer phase diagram is expected³²⁻⁴⁰.

In the present manuscript, we study the commensurate-incommensurate transitions of the hard-core boson ladder with equal densities in the two legs, while varying interleg coupling and flux⁴¹, now tuning the filling to different values. We confirm that above a threshold in the interleg coupling an enlargement of the Meissner phase occurs⁴⁰ while below the threshold the commensurate-incommensurate phase transition³ to the vortex phase takes place. However, within the vortex phase we find that a second incommensuration manifests at a flux commensurate with the filling, which we characterize by different observables, extending to different fillings ($\rho < 1$) the previous analysis⁴¹.

The paper is organized as follows. In Sec. I, we present the model and the Hamiltonian and define the observables. In Sec. II we describe the bosonization treatment, the Meissner state and the commensurate-incommensurate (C-IC) transition. Here we also give a description of the C-IC transition in terms of a fermionization approach, gaining additional insight on the physics of the problem. In Sec. III, we discuss the second incommensuration as a function of the filling. Finally, in the conclusion we present the phase-diagram emerging for the half-filled case.

I. MODEL AND HAMILTONIAN

The lattice Hamiltonian of the bosonic ladder in a flux^{2,3} reads:

$$H_\lambda = \sum_{j,\sigma} -t(b_{j,\sigma}^\dagger e^{i\lambda\sigma} b_{j+1,\sigma} + b_{j+1,\sigma}^\dagger e^{-i\lambda\sigma} b_{j,\sigma}) - \Omega \sum_{j,\sigma} b_{j,\sigma}^\dagger b_{j,-\sigma}, \quad (1)$$

where the operator $b_{j,\sigma}^{(\dagger)}$ destroys (creates) a hard core boson on site j of the σ chain. We have defined $\sigma = \pm 1/2$ as the chain index^{3,41}, λ as the flux in each plaquette (corresponding to a Landau gauge with the vector potential parallel to the legs), Ω as the interchain hopping. The $tb_{j,\sigma}^\dagger e^{i\lambda\sigma}$ is the hopping amplitude on the chain σ . This hard-core boson model can be mapped into a spin-ladder model with Dzialoshinskii-Moriya interactions^{42,43}, as detailed in Appendix A. As a result of translational invariance and parity, the spectrum of the Hamiltonian (1) is even and 2π -periodic in λ .

The leg and rung currents are now defined: the leg-current operator $J_\parallel(j, \lambda)$ is

$$J_\parallel(j, \lambda) = \sum_{\sigma} -it\sigma(b_{j,\sigma}^\dagger e^{i\lambda\sigma} b_{j+1,\sigma} - b_{j+1,\sigma}^\dagger e^{-i\lambda\sigma} b_{j,\sigma}), \quad (2)$$

and the rung current is

$$J_\perp(j) = -i\Omega(b_{j,\uparrow}^\dagger b_{j\downarrow} - b_{j,\downarrow}^\dagger b_{j\uparrow}). \quad (3)$$

Where the expectation value of the leg-current $\langle J_\parallel(\lambda) \rangle$ is odd and 2π -periodic in λ . The average densities of bosons are $\rho_\sigma = \frac{N_\sigma}{L}$ where N_σ is the number of σ particles and L is the length of the chain. In the rest of the manuscript, we will be considering a fixed total density $\rho = \rho_\uparrow + \rho_\downarrow$. In the absence of applied flux λ the ground state of the system is a rung-Mott Insulator for $\rho = 1$ and a superfluid for $\rho < 1$ ⁴⁴. This situation is not changed at finite λ so that for $\rho = 1$ Mott-Meissner and Mott-Vortex phase^{12,13,40} are obtained.

We will consider the following observables: the rung-current correlator $C(k)$

$$C(k) = \sum_j \langle J_\perp(j) J_\perp(0) \rangle e^{-ikj}, \quad (4)$$

the symmetric density correlator $S_c(k)$

$$S_c(k) = \sum_{j,\sigma,\sigma'} \langle n_{j,\sigma} n_{0,\sigma'} \rangle e^{-ikj}, \quad (5)$$

the antisymmetric density correlator $S_s(k)$

$$S_s(k) = \sum_{j,\sigma,\sigma'} \sigma\sigma' \langle n_{j,\sigma} n_{0,\sigma'} \rangle e^{-ikj}, \quad (6)$$

and the spin-resolved momentum distribution $n_\sigma(k)$

$$n_\sigma(k) = \sum_j \langle b_{j,\sigma}^\dagger b_{0,\sigma} \rangle e^{-ikj}. \quad (7)$$

The non spin-resolved momentum distribution is $n(k) = n_\uparrow(k) + n_\downarrow(k)$.

II. BOSONIZATION OF THE TWO-LEG BOSON LADDER

We apply Haldane's bosonization of interacting bosons⁴⁵ to the Hamiltonian (1) assuming that Ω is a perturbation. In the absence of interchain couplings and spin-orbit coupling, the Hamiltonian of the bosons can be written as:

$$H_0 = \sum_{\sigma} \int \frac{dx}{2\pi} \left[u_{\sigma} K_{\sigma} (\pi \Pi_{\sigma})^2 + \frac{u_{\sigma}}{K_{\sigma}} (\partial_x \phi_{\sigma})^2 \right], \quad (8)$$

where $[\phi_{\alpha}(x), \Pi_{\beta}(x')] = i\delta_{\alpha\beta}\delta(x-x')$, u_{σ} is the velocity of excitations, K_{σ} is the Tomonaga-Luttinger (TL) exponent. In the case of hard-core bosons, $u_{\sigma} = 2t \sin(\pi\rho_{\sigma}^0)$ and $K_{\sigma} = 1$.

Introducing the fields $\theta_{\alpha} = \pi \int^x \Pi_{\alpha}$, we can represent⁴⁵ the boson annihilation operators as:

$$\frac{b_{j\sigma}}{\sqrt{a}} = \psi_{\sigma}(x) = e^{i\theta_{\sigma}(x)} \sum_{m=0}^{+\infty} A_m^{(\sigma)} \cos(2m\phi_{\sigma}(x) - 2m\pi\rho_{\sigma}^{(0)}x), \quad (9)$$

and the density operators⁴⁵ as:

$$\frac{n_{j\sigma}}{a} = \rho_{\sigma}(x) = \rho_{\sigma}^{(0)} - \frac{1}{\pi} \partial_x \phi_{\sigma} + \sum_{m=1}^{\infty} B_m^{(\sigma)} \cos(2m\phi_{\sigma}(x) - 2m\pi\rho_{\sigma}^{(0)}x). \quad (10)$$

Here, we have introduced the lattice spacing a , while A_m and B_m are non-universal coefficients. In the case of hard core bosons at half filling, these coefficients have been found analytically⁴⁶. From Eq.(9), we deduce the bosonized expression of the interchain hopping as:

$$-\Omega A_0^2 \int dx \cos(\theta_{\uparrow} - \theta_{\downarrow}), \quad (11)$$

where we have kept only the most relevant term in the renormalization group sense³. Till now, we haven't considered the effect of the flux λ . We now show that it can be exactly incorporated in the bosonized Hamiltonian. In the absence of interchain hopping Ω , we can perform independent gauge transformations on the upper and the lower leg of the ladder. In particular, the gauge transformation:

$$b_{j,\sigma} = e^{-i\lambda\sigma j} \bar{b}_{j,\sigma} \quad (12)$$

entirely removes λ from the Hamiltonian. We can then apply the Haldane bosonization (8)–(9) to the $\bar{b}_{j,\sigma}$ operators. Combining the resulting expressions with Eq. (12), we see that $b_{j,\sigma}$ has now a bosonized expression of the form:

$$\frac{b_{j\sigma}}{\sqrt{a}} = \psi_{\sigma}(x) = e^{i\bar{\theta}_{\sigma}(x) - i\sigma \frac{\lambda x}{a}} \sum_{m=0}^{+\infty} A_m^{(\sigma)} \cos(2m\bar{\phi}_{\sigma}(x) - 2m\pi\rho_{\sigma}^{(0)}x). \quad (13)$$

The Hamiltonian now reads:

$$H = \sum_{\sigma} \int \frac{dx}{2\pi} \left[u_{\sigma} K_{\sigma} (\pi \bar{\Pi}_{\sigma})^2 + \frac{u_{\sigma}}{K_{\sigma}} (\partial_x \bar{\phi}_{\sigma})^2 \right], \quad (14)$$

and the bosonized expression of the density remains unchanged. The boson operators $b_{j,\sigma}$ can be written in the form (9) with $\phi_{\sigma} = \bar{\phi}_{\sigma}$ and $\theta_{\sigma}(x) = \bar{\theta}_{\sigma}(x) - \sigma \frac{\lambda x}{2a}$ and the Hamiltonian expressed in terms of the fields Π_{σ} and ϕ_{σ} becomes:

$$H = \sum_{\sigma} \int \frac{dx}{2\pi} \left[u_{\sigma} K_{\sigma} \left(\pi \Pi_{\sigma} + \sigma \frac{\lambda}{a} \right)^2 + \frac{u_{\sigma}}{K_{\sigma}} (\partial_x \bar{\phi}_{\sigma})^2 \right], \quad (15)$$

Since $u_{\uparrow} = u_{\downarrow}$ and $K_{\uparrow} = K_{\downarrow}$, it is convenient to introduce the symmetric and antisymmetric representation:

$$\Pi_c = \frac{1}{\sqrt{2}}(\Pi_{\uparrow} + \Pi_{\downarrow}) \quad \Pi_s = \frac{1}{\sqrt{2}}(\Pi_{\uparrow} - \Pi_{\downarrow}) \quad (16)$$

$$\phi_c = \frac{1}{\sqrt{2}}(\phi_{\uparrow} + \phi_{\downarrow}) \quad \phi_s = \frac{1}{\sqrt{2}}(\phi_{\uparrow} - \phi_{\downarrow}), \quad (17)$$

in order to rewrite (8)– (11) as:

$$H = H_c + H_s \quad (18)$$

$$H_c = \int \frac{dx}{2\pi} \left[u_c K_c (\pi \Pi_c)^2 + \frac{u_c}{K_c} (\partial_x \phi_c)^2 \right] \quad (19)$$

$$H_s = \int \frac{dx}{2\pi} \left[u_s K_s (\pi \Pi_s)^2 + \frac{u_s}{K_s} (\partial_x \phi_s)^2 \right] - \Omega A_0^2 \int dx \cos(\sqrt{2}\theta_s). \quad (20)$$

The Hamiltonian H_c describes the gapless charge modes, while H_s represents a quantum sine-Gordon model^{47–49}. As discussed in³, when $\Omega \neq 0$ the λ term is imposing a gradient of $\theta_\uparrow - \theta_\downarrow$, while the term (11) is imposing a constant value of $\theta_\uparrow - \theta_\downarrow$. For sufficiently large values of λ it becomes energetically advantageous to populate the ground state with solitons giving rise to an incommensurate phase. In the ladder language, such incommensurate phase is the vortex lattice.

A. Gapful excitations in the Meissner state

The quantum sine-Gordon model (20) is integrable^{50,51} and its spectrum is fully determined. The Hamiltonian (20) has a gap $\Delta_s \sim \frac{u_s}{a} |a\Omega/u_s|^{\frac{2K_s}{4K_s-1}}$ for $K_s > 1/4$. In its ground state $\langle \theta_s \rangle \equiv 0[\pi\sqrt{2}]$. For $1/4 < K_s < 1/2$, the excitations above the ground state are solitons and antisolitons with the Lorentz-invariant dispersion $E_s(k) = \sqrt{(u_s k)^2 + \Delta_s^2}$. The soliton and the antisoliton are topological excitations of the field θ_s that carry a leg current $j_s^z = \pm u_s K_s$. In the case where one is considering the gap between the ground state and an excited state of total spin current zero (i. e. containing at least one soliton and one antisoliton), the measured gap will be $2\Delta_s$. When $K_s > 1/2$, the solitons⁴⁸ and the antisolitons attract each other and can form bound states called breathers that do not carry any spin current. The measured gap between the ground state and the lowest zero current state will be the mass of the lightest breather⁵²

$$\Delta_s = \frac{4u_s}{\alpha\sqrt{\pi}} \frac{\Gamma\left(\frac{1}{8K_s-2}\right) \sin\left(\frac{\pi}{8K_s-2}\right)}{\Gamma\left(\frac{2K_s}{4K_s-1}\right)} \left[\frac{\pi\Gamma\left(1 - \frac{1}{4K_s}\right) \Omega A_0^2}{\Gamma\left(\frac{1}{4K_s}\right) 2u} \right]^{\frac{2K_s}{4K_s-1}}. \quad (21)$$

In the case of hard core bosons⁵³, which is the one considered in the numerical analysis here, we have $K_c = K_s = 1$, so $\Delta_s \sim \Omega^{2/3}$. In that limit, the Hamiltonian (20) has been studied in relation with spin-1/2 chain materials with staggered Dzialoshinskii-Moriya in a magnetic field^{54–59}. With a weak spin-spin repulsion logarithmic corrections^{54,55} are actually obtained as a result a marginal flow, and $\Delta_s \sim \Omega^{2/3} |\ln \Omega|^{1/6}$. Without this spin-spin interaction, a quantitative estimate of the gap can be obtained from the results of^{52,60}:

$$\Delta_s = \frac{u_s}{\alpha} \frac{2\Gamma(1/6)}{\sqrt{\pi}\Gamma(2/3)} \left(\frac{\pi\Gamma(3/4) \Omega A_0^2 \alpha^2}{\Gamma(1/4) 2u_s} \right)^{2/3}. \quad (22)$$

Besides the solitons and antisolitons, there are two breathers^{61–63}, a light breather of mass Δ_s and a heavy breather of mass $\sqrt{3}\Delta_s$.

The amplitude A_0 can be estimated for hard core bosons in the case of low density, using the continuum limit^{64,65} or in the case of half-filling⁴⁶. In the first case,

$$\frac{A_0^2 \alpha}{2} = \frac{G(3/2)^4 n_0^{1/2}}{\sqrt{2\pi}}, \quad (23)$$

where G is the Barnes G function and n_0 is the number of particles per site. In the second case,

$$\frac{A_0^2 \alpha}{2} = \frac{2C_0}{\sqrt{\pi}} \simeq 0.588352. \quad (24)$$

This gives the estimates:

$$\Delta_s = \frac{u_s}{\alpha} \frac{2\Gamma(1/6)}{\sqrt{\pi}\Gamma(2/3)} \left(\frac{\sqrt{\pi}\Gamma(3/4)G(3/2)^4 \Omega \alpha}{\sqrt{2}\Gamma(1/4) u_s} \right)^{2/3} n_0^{1/3}, \quad (25)$$

for low density, and:

$$\Delta_s = \frac{u_s}{\alpha} \frac{2\Gamma(1/6)}{\sqrt{\pi}\Gamma(2/3)} \left(\frac{2\sqrt{\pi}\Gamma(3/4)C_0}{\Gamma(1/4)} \frac{\Omega\alpha}{u_s} \right)^{2/3}, \quad (26)$$

for half-filling.

B. Correlation functions in the Meissner state

As for $K_s > 1/4$ the ground state of H_s has θ_s long-range ordered and the excitations above the ground state are gapped, the system described by (18) is a Luther-Emery liquid⁶⁶. In such a phase,

$$b_{j,\sigma} \sim \langle e^{i\sigma\sqrt{2}\theta_s(ja)} \rangle e^{i\frac{\theta_s(ja)}{\sqrt{2}}}, \quad (27)$$

giving rise to correlations $\langle b_{j,\sigma} b_{j,\sigma'} \rangle \sim \frac{|\langle \cos(\theta_s(ja)/\sqrt{2}) \rangle|^2}{|j-j'|^{1/(4K_c)}}$. This behavior is a remnant of the single condensate obtained in the non-interacting case^{31,32}. Since

$$J_{\perp} = \Omega A_0^2 \sin \sqrt{2}\theta_s, \quad (28)$$

we have $\langle J_{\perp}(x) \rangle = 0$ and

$$\langle J_{\perp}(x) J_{\perp}(x') \rangle \sim e^{-|x-x'|/\xi}, \quad (29)$$

as $|x-x'| \rightarrow \infty$. Thus, the average rung-current vanishes and its fluctuations are short ranged and commensurate, so that $C(k)$ takes a Lorentzian shape in the vicinity of $k=0$.

In the case of density-density and spin-spin correlation functions, we have:

$$\frac{1}{a} \sum_{\sigma} n_{j,\sigma} \sim \rho^{(0)} - \frac{\sqrt{2}}{\pi} \partial_x \phi_c + \sum_m B_m \cos(m\sqrt{2}\phi_c - \pi m \rho^{(0)} x) \cos(m\sqrt{2}\phi_s), \quad (30)$$

and

$$\frac{1}{2a} \sum_{\sigma} \sigma n_{j,\sigma} \sim \rho^{(0)} - \frac{1}{\pi\sqrt{2}} \partial_x \phi_s + \sum_m B_m \cos(m\sqrt{2}\phi_c - \pi m \rho^{(0)} x) \sin(m\sqrt{2}\phi_s). \quad (31)$$

Since the field θ_s is long-range ordered, exponentials $e^{i\beta\phi_s}$ and derivatives $\partial_x^n \phi_s$ of its dual field ϕ_s are short-range ordered. As a result, the density correlations decay as $(x-x')^{-2}$ at long distance leading to $S_c(k) = K_c |k| / (2\pi)$, while the spin-spin correlations are decaying exponentially giving a Lorentzian shape for $S_s(k)$. Finally, if we consider the longitudinal spin current, the obtained bosonized expression is:

$$J_{\parallel}(\lambda) = \frac{u_s K_s}{\sqrt{2}} \left(\Pi_s + \frac{\lambda}{\pi a \sqrt{2}} \right). \quad (32)$$

In the Meissner phase, the characterizing $\alpha \lambda$ behavior is obtained as $\langle J_{\parallel}(\lambda) \rangle = \lambda u_s K_s (2\pi a)^{-1}$.

C. Commensurate-Incommensurate transition

Adding the spin-orbit coupling λ in (20) gives a Hamiltonian for the spin modes:

$$H_s = \int \frac{dx}{2\pi} \left[u_s K_s \left(\pi \Pi_s + \frac{\lambda}{\sqrt{2}a} \right)^2 + \frac{u_s}{K_s} (\partial_x \phi_s)^2 \right] - \Omega A_0^2 \int dx \cos \sqrt{2}\theta_s. \quad (33)$$

Expanding $(\pi \Pi_s + \lambda/\sqrt{2}a)^2$ and using the fact that $\pi \Pi_s = \partial_s \theta_s$, we see that up to a constant, the spin orbit coupling adds a term:

$$+ \frac{u_s K_s \lambda}{a \sqrt{2}} \int \frac{dx}{\pi} \partial_x \theta_s. \quad (34)$$

Now, if we consider the sine-Gordon Hamiltonian (20), calling N_s is the number of solitons and $N_{\bar{s}}$ the number of antisolitons, we have:

$$N_s - N_{\bar{s}} = \int_{-\infty}^{\infty} \frac{dx}{\pi\sqrt{2}} \partial_x \theta_s, \quad (35)$$

and the contribution of the spin-orbit coupling is simply

$$\frac{u_s K_s \lambda}{a} (N_s - N_{\bar{s}}). \quad (36)$$

Meanwhile, the cost of forming N_s solitons and $N_{\bar{s}}$ antisolitons is $\Delta_s(N_s + N_{\bar{s}})$. When $|\lambda| > \lambda_c = \frac{a\Delta_s}{u_s K_s}$, there is an energy gain to create solitons (or antisolitons) in the ground state. Because of the repulsion between solitons, their density remains finite, and we obtain another Luttinger liquid. This is the commensurate-incommensurate transition^{5-7,67}.

In the incommensurate (IC) phase, the Hamiltonian describing the Luttinger liquid of solitons is:

$$H = \int \frac{dx}{2\pi} \left[u_s^*(\lambda) K_s^*(\lambda) (\pi \hat{\Pi}_s)^2 + \frac{u_s^*(\lambda)}{K_s^*(\lambda)} (\partial_x \phi_s)^2 \right], \quad (37)$$

with $\theta_s = \hat{\theta}_s - \text{sign}(\lambda)q(\lambda)x/\sqrt{2}$. The density of solitons is proportional to $q(\lambda)$, while $u_s^*(\lambda)$ is the renormalized velocity of excitations and $K_s^*(\lambda)$ is the renormalized Luttinger exponent.

We now address the behavior of the observables in the IC phase. Near the transition^{7,68}, for $\lambda \rightarrow \lambda_c + 0$, $K_s^*(\lambda) \rightarrow 1/2$, $q(\lambda) \propto \sqrt{\lambda - \lambda_c}$ and $u_s^*(\lambda) \propto \sqrt{\lambda - \lambda_c}$. The expression of the spin current in the IC phase now becomes:

$$\langle J_{\parallel}(\lambda) \rangle = \frac{u_s K_s}{2} \left(\frac{\lambda}{\pi a} - \text{sign}(\lambda)q(\lambda) \right), \quad (38)$$

namely the existence of a finite soliton density reduces the average spin current. This justifies the interpretation of these solitons as vortices letting the current to flow along the legs. For large λ we have $q(\lambda) \sim |\lambda|/(\pi a)$ so that the expectation value of the spin current eventually vanishes for large flux values.

Let us turn to the momentum distribution. In the IC phase and for finite size L with periodic boundary conditions one has:

$$\langle b_{j,\sigma}^\dagger b_{j,\sigma'} \rangle = \frac{e^{i\sigma q(\lambda)(x-x')} \delta_{\sigma\sigma'}}{\left[\frac{L}{\pi} \sin \left(\frac{\pi|x-x'|}{L} \right) \right]^{1/(4K_c)+1/(4K_s^*)}}. \quad (39)$$

As a result, for $1/(4K_c) + 1/(4K_s^*) < 1$ one has:

$$n_\sigma(k) = 2 \left(\frac{L}{2\pi} \right)^{1-\frac{1}{4K_c}-\frac{1}{4K_s^*}} \frac{\Gamma \left(1 - \frac{1}{4K_c} - \frac{1}{4K_s^*} \right) \cos \left(\frac{\pi}{8K_c} + \frac{\pi}{8K_s^*} \right) \Gamma \left(\frac{1}{8K_c} + \frac{1}{8K_s^*} + \frac{L|k-\sigma q(\lambda)|}{2\pi} \right)}{\Gamma \left(1 - \frac{1}{8K_c} - \frac{1}{8K_s^*} + \frac{L|k-\sigma q(\lambda)|}{2\pi} \right)}, \quad (40)$$

so that now $n_\sigma(k)$ gets a peak for $k = \sigma q(\lambda)$, whose height scales as $L^{1-1/(4K_c)-1/(4K_s^*)}$. Comparing with the non-interacting case³¹, the power-law divergences are the remnant of the Bose condensate³² formed at $k = 0$ in the Meissner phase or at $k = \pm q(\lambda)/2$ in the vortex phase.

Turning to the spin-current correlation function, in the IC phase we have^{3,4}:

$$\langle J_{\perp}(j) J_{\perp}(j') \rangle \sim \frac{\cos[q(\lambda)(x-x')]}{\left[\frac{L}{\pi} \sin \frac{\pi|j-j'|}{L} \right]^{\frac{1}{K_s^*}}}. \quad (41)$$

Since $1/2 \leq K_s^* \leq 1$, the correlation function $C(k)$ presents in the IC phase two cusps at $k = \pm q(\lambda)$.

Turning now to the density correlation function, we have:

$$\left\langle \sum_{\sigma,\sigma'} n_{j,\sigma} n_{0,\sigma'} \right\rangle \sim -\frac{2K_c}{L^2 \sin^2 \left(\frac{\pi j}{L} \right)} + \frac{\cos(\pi \rho^{(0)} j)}{\left[\frac{L}{\pi} \sin \left(\frac{\pi j}{L} \right) \right]^{K_c+K_s^*}}, \quad (42)$$

$$\left\langle \sum_{\sigma,\sigma'} \sigma \sigma' n_{j,\sigma} n_{0,\sigma'} \right\rangle \sim -\frac{K_s}{2L^2 \sin^2 \left(\frac{\pi j}{L} \right)} + \frac{\cos(\pi \rho^{(0)} j)}{\left[\frac{L}{\pi} \sin \left(\frac{\pi j}{L} \right) \right]^{K_c+K_s^*}}. \quad (43)$$

Since $1 \leq K_c + K_s^* \leq 2$, we find that both $S_s(k)$ and $S_c(k)$ possess cusp singularities $S_{c/s}(k) \sim S_{c/s}(\pi\rho^0) + C_{c/s}|k - \pi\rho^{(0)}|^{K_c+K_s^*-1}$ in the vicinity of $k = \pi\rho^{(0)}$ in the vortex phase, with evident notation for the subscript c/s . In the hard core boson system, with $K_c = K_s^* = 1$, the cusp singularities become slope discontinuities.

Moreover, the behaviors $S_c(k) \sim \frac{2K_c|k|}{\pi}$ and $S_s(k) \sim \frac{K_s|k|}{2\pi}$ as $k \rightarrow 0$ signal that both charge and spin excitations are gapless in the vortex phase.

We performed numerical simulations for the hard-core spinless bosons on a two-leg ladder as a function of flux and interchain hopping and for different fillings by means of DMRG simulations^{69,70} with Periodic Boundary Conditions (PBC). Simulations are performed for sizes up to $L = 64$, keeping up to $m = 1256$ states during the renormalization procedure. The truncation error, that is the weight of the discarded states, is at most of order 10^{-6} , while the error on the ground-state energy is of order 5×10^{-5} at most.

A summary for the behavior of observables and correlation functions across the commensurate-incommensurate transition at two different fillings is shown in Fig. 1 for $\rho = 0.75$ and in Fig. 2 for $\rho = 0.5$. In each panel a) of the two figures we compare the behavior of the Fourier Transform (FT) of the rung-current correlation function $C(k)$ in the Meissner phase in the Vortex phase. The numerical data confirm the prediction of a structureless shape in the Meissner phase and the appearance of two cusp-like peaks in the Vortex phase, respectively at $k = q(\lambda)$ and $k = 2\pi - q(\lambda)$. Since we shown data in the vortex phase far from the transition $q(\lambda) = \lambda$, as expected. The spin gap closes in the Vortex phase, which is traceable also in the low-momentum behavior of the spin static structure factor $S_s(k)$ displayed in each panel b) of the two figures: in the Vortex phase $S_s(k) = K_s|k|/2\pi$ while in the Meissner phase $S_s(k) = S_s(0) + ak^2$ with $S_s(0) > 0$. In these cases $K_s = 1$ as expected for a hard-core boson system. At large momenta the Lorentzian profile centered at $k = \pi$, characteristic of the Meissner phase, is replaced by two slope discontinuities at $k = \pi\rho$ and $k = 2\pi - \pi\rho$ as expected in the Vortex phase for $K_s = K_c = 1$. The same evolution can be seen in the charge static structure factors shown in the c) panels of Figs.1 and 2. The commensurate-incommensurate transition is clearly visible in the momentum distribution here shown in panels d) of Figs.1 and 2: the Meissner phase shows up with only one cusp-like peak at $k = 0$ as expected in a bosonic Tomonaga-Luttinger liquid, while the Vortex phase is characterized by two peaks with same shape, centered at $k = \pm q(\lambda)/2$.

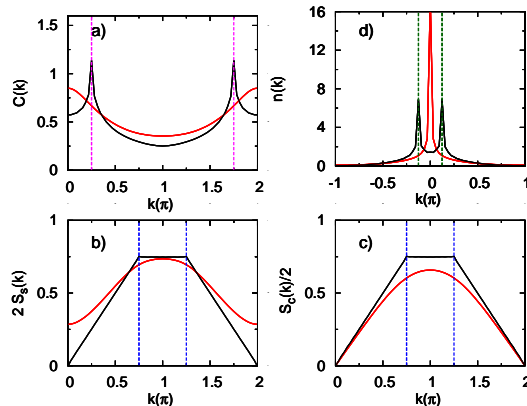


FIG. 1: First incommensuration: appearance of the standard Vortex phase. DMRG simulation for $L = 64$ in PBC for $\lambda = \pi/4$ and $\rho = 0.75$ ($\lambda = \rho\pi$). FT of the correlation functions described in the text for two different values of interchain coupling $\Omega = 0.0625$ (black solid line) and 0.5 (red solid line), respectively in the Vortex and Meissner phase. Panel a): rung-current correlation function $C(k)$. Panel b): spin correlation function $S_s(k)$. Panel c): twice the charge correlation function $2S_c(k)$. Panel d): total momentum distribution $n(k)$. See text for the corresponding definitions. The blue dashed lines in panels b) and c) signal the values $k = \pi\rho$ and $k = 2\pi - \pi\rho$. The magenta dashed lines in panel a) signals the peaks positions of $C(k)$, $k = \lambda$ and $k = 2\pi - \lambda$. The dark-green dashed lines in panel d) signals the peaks of the momentum distribution at $k = \pm\lambda/2$.

D. Fermionization approach

For $K_s = 1/2$, the sine-Gordon Hamiltonian (33) can be rewritten as a free fermion Hamiltonian^{47,66} allowing a more detailed treatment of the commensurate-incommensurate transition^{3,5}. Such a treatment sheds additional light on the physics of this commensurate-incommensurate transition, providing an overall alternative description considering that no differences are expected at a qualitative level away from the $K_s = 1/2$ case.

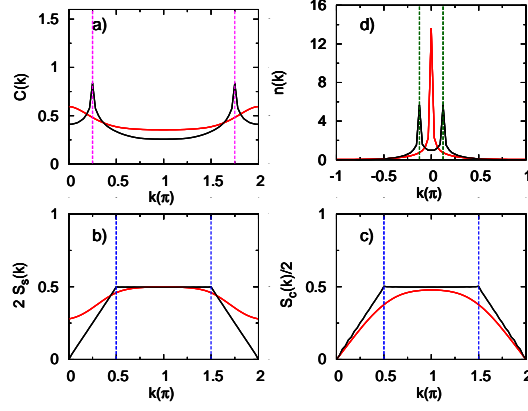


FIG. 2: The same as in Fig. 1 for $\rho = 0.5$.

We have:

$$H_s = -iu_s \int dx (\psi_R^\dagger \partial_x \psi_R - \psi_L^\dagger \partial_x \psi_L) - h \int dx (\psi_R^\dagger \psi_R + \psi_L^\dagger \psi_L) - m \int dx (\psi_R^\dagger \psi_L + \psi_L^\dagger \psi_R), \quad (44)$$

where $m = \pi\Omega A_0^2 a$, $h = \frac{\lambda u_s}{2a}$ and the fermion annihilation operators $\psi_{R,L}^\dagger$ are destroying the solitons. The detailed correspondence between the fermionic and bosonic expression of the lattice operators is reported in the Appendix B.

In the fermionic representation (44), the Hamiltonian is readily diagonalized in the form

$$H = \sum_{k,r=\pm} (r\sqrt{(u_s k)^2 + m^2} - h) c_{k,r}^\dagger c_{k,r}, \quad (45)$$

by writing:

$$\begin{pmatrix} \psi_R(x) \\ \psi_L(x) \end{pmatrix} = \frac{1}{\sqrt{L}} \sum_k e^{ikx} \begin{pmatrix} \cos \varphi_k & -\sin \varphi_k \\ \sin \varphi_k & \cos \varphi_k \end{pmatrix} \begin{pmatrix} c_{k+} \\ c_{k-} \end{pmatrix}, \quad (46)$$

with: $e^{2i\varphi_k} = \frac{uk+im}{\sqrt{(uk)^2+m^2}}$. The commensurate phase⁵ is obtained for $|h| < |m|$ and the incommensurate phase for $|h| > |m|$.

We can express the currents as:

$$J_{\parallel}(\lambda) = \frac{u_s}{2} \left[\frac{\lambda}{2\pi a} - (\psi_R^\dagger \psi_R + \psi_L^\dagger \psi_L) \right], \quad (47)$$

$$J_{\perp}(\lambda) = i\sqrt{2}m(\psi_R^\dagger \psi_L - \psi_L^\dagger \psi_R), \quad (48)$$

and the $q \sim 0$ component of $n_{j\uparrow} - n_{j\downarrow}$ as:

$$(n_{j\uparrow} - n_{j\downarrow})_{q \sim 0} \sim \psi_R^\dagger \psi_R - \psi_L^\dagger \psi_L. \quad (49)$$

Using (47), one has³ $\langle J_{\parallel} \rangle = \frac{u_s \lambda}{4\pi a}$ in the commensurate phase, and

$$\langle J_{\parallel} \rangle = \frac{u_s}{4\pi a} \left[\lambda - \sqrt{\lambda^2 - \lambda_c^2} \right] \quad (50)$$

in the incommensurate phase. The finite-size scaling of the leg current has been derived in⁷¹. As $\langle \psi_R^\dagger \psi_L \rangle$ is real (see Appendix B), the average rung current vanishes.

However, rung-current fluctuations are non-vanishing. Indeed, with the help of Wick's theorem we obtain:

$$\langle J_{\perp}(x) J_{\perp}(x') \rangle \propto \left[\langle \psi_R^\dagger(x) \psi_L(x') \rangle \langle \psi_R^\dagger(x') \psi_L(x) \rangle + \langle \psi_L^\dagger(x) \psi_R(x') \rangle \langle \psi_L^\dagger(x') \psi_R(x) \rangle \right. \quad (51)$$

$$\left. - \langle \psi_R^\dagger(x) \psi_R(x') \rangle \langle \psi_L^\dagger(x') \psi_L(x) \rangle - \langle \psi_L^\dagger(x) \psi_L(x') \rangle \langle \psi_R^\dagger(x') \psi_R(x) \rangle \right]. \quad (52)$$

In the commensurate phase, the correlators in (51) can be evaluated using (46). Referring to Appendix B for details, one obtains:

$$\langle J_{\perp}(x)J_{\perp}(x') \rangle \propto \left(\frac{m}{2\pi u_s} \right)^2 \left[K_0 \left(\frac{m|x-x'|}{u_s} \right)^2 + K_1 \left(\frac{m|x-x'|}{u_s} \right)^2 \right], \quad (53)$$

where K_0 and K_1 are the modified Bessel functions. The exponential decay is thus recovered for $|x-x'| \gg u/m$. Taking the Fourier transform, we find

$$C(0) - C(k) \propto E \left(-\frac{(uk)^2}{(2m)^2} \right) - K \left(-\frac{(uk)^2}{(2m)^2} \right), \quad (54)$$

where E and K are complete elliptic integrals⁷². Using the fermion representation, we can also show that:

$$S_s(0) - S_s(k) \sim \pi - E \left(-\frac{(uk)^2}{(2m)^2} \right). \quad (55)$$

In the incommensurate phase, the fermion correlation functions are expressible instead in terms of incomplete Bessel functions⁷³. The detailed expressions are reported in the Appendix B). For large distances, $|x-x'| \gg u/m$, we can neglect the contribution from the lower band. The contribution from the upper band can be obtained from the asymptotic expansions given in Ref. 73. In the limit $uk_F \gg m$, simple physical arguments give:

$$\langle J_{\perp}(x)J_{\perp}(x') \rangle \sim \frac{\cos 2k_F(x-x')}{4\pi^2(x-x')^2} + \dots, \quad (56)$$

so the Fermi wavevector $k_F = \sqrt{h^2 - m^2}/u_s = q(\lambda)/2$. Taking the Fourier transform (56), we deduce that $C(k)$ has slope discontinuities at $k = \pm 2k_F$. By contrast, in that limit, we find that $\langle (n_{j\uparrow} - n_{j\downarrow})(n_{j'\uparrow} - n_{j'\downarrow}) \rangle \sim (j-j')^2$ as expected from the bosonization arguments.

III. THE SECOND INCOMMENSURATION APPEARING AT $\lambda \simeq \pi\rho$

As λ gets close to $\pi\rho$, with $\rho = N/L$ is the density per rung and for N/L not small compared to unity, $\lambda u_s/a$ becomes of the order of the energy cutoff u_s/a and the form (33) for the Hamiltonian cannot be used. In order to describe the low-energy physics at $\lambda = \rho\pi$, it is necessary to choose a gauge with the vector potential along the rungs of the ladder, so that the interchain hopping reads:

$$H_{hop} = \Omega \sum_{j,\sigma} e^{i2\pi\sigma(\frac{N}{L})j} b_{j,\sigma}^{\dagger} b_{j,-\sigma}. \quad (57)$$

Applying bosonization to (57), we obtain from (9) the following representation for the interchain hopping:

$$H_{hop} = \frac{\Omega}{2\pi a} \int dx e^{i\sqrt{2}\phi_c} \left[e^{-i\sqrt{2}(\theta_s + \phi_s)} + e^{-i\sqrt{2}(\theta_s - \phi_s)} \right] + e^{-i\sqrt{2}\phi_c} \left[e^{i\sqrt{2}(\theta_s + \phi_s)} + e^{i\sqrt{2}(\theta_s - \phi_s)} \right]. \quad (58)$$

The latter can be rewritten in terms of $SU(2)_1$ Wess-Zumino-Novikov-Witten (WZNW) currents⁷⁴:

$$H_{hop} = \Omega \int dx \left[i e^{i\sqrt{2}\phi_c} (J_R^- + J_L^-) + \text{H. c.} \right]. \quad (59)$$

In the case of $N/L = 1$, the complex exponential is replaced by a cosine⁴¹. At commensurate fillings, N/L is rational and a term $\cos m\sqrt{2}\phi_c$ is also present in the Hamiltonian. In the presence of such term, the symmetry of the $U(1)$ charge Hamiltonian is lowered to \mathbb{Z}_m and a spontaneous symmetry breaking giving rise to a charge gap and a long-range ordered $e^{i\sqrt{2}\phi_c}$ becomes possible. At generic filling, we have an unbroken $U(1)$ symmetry $\phi_c \rightarrow \phi_c + \alpha$ and $\theta_s \rightarrow \theta_s - \alpha$. In such case, the Mermin-Wagner theorem^{75,76} precludes long range ordering for $\phi_c - \theta_s$. However, since the perturbation in (59) has non-zero conformal spin, it is still expected to give rise to incommensurate correlations. To form a qualitative idea of such incommensuration, we will use a mean-field treatment. Assuming $\langle \phi_c \rangle = 0$, the Hamiltonian $H_c + H_s + H_{hop}$ can be treated in mean-field theory⁷⁷⁻⁸⁰. After defining :

$$\begin{aligned} \frac{g_c}{\pi a} &= 8\Omega \langle J_R^y + J_L^y \rangle_{s,MF}, \\ h_s &= 8\Omega \langle \cos \sqrt{2}\phi_c \rangle_{c,MF}, \end{aligned} \quad (60)$$

using a $\pi/2$ rotation around the x axis, $J_\nu^y = \tilde{J}_\nu^z$, $J_\nu^z = -\tilde{J}_\nu^y$, and applying abelian bosonization⁸¹, we rewrite:

$$H_s^{MF} = \int \frac{dx}{2\pi} u_s \left[(\pi \tilde{\Pi}_s)^2 + (\partial_x \tilde{\phi}_s)^2 \right] - \frac{h_s}{\pi \sqrt{2}} \int \partial_x \tilde{\phi}_s dx, \quad (61)$$

which allows us to write:

$$-\frac{1}{\pi \sqrt{2}} \langle \partial_x \tilde{\phi}_s \rangle = \sum_{\nu=R,L} \langle \tilde{J}_\nu^z \rangle = \langle J_R^y + J_L^y \rangle = -\frac{h_s}{2\pi u_s}. \quad (62)$$

In turn, this allows us to solve (60) with $h_s \sim \Omega^2$ and $g_c \sim \Omega^3$. We obtain a gap in the total density excitations, $\Delta_c \sim \Omega^2$, while the antisymmetric modes remain gapless and develop an incommensuration. To characterize the incommensuration, we first make a shift of the field $\tilde{\phi}_s \rightarrow \tilde{\phi}_s + \frac{h_s x}{u_s \sqrt{2}}$ while $\tilde{\theta}_s \rightarrow \tilde{\theta}_s$, thus

$$\sin \sqrt{2} \tilde{\theta}_s = \sin \sqrt{2} \tilde{\theta}_s \quad (63)$$

$$\cos \sqrt{2} \tilde{\theta}_s = \sin \left(\sqrt{2} \tilde{\phi}_s + \frac{h_s x}{u_s} \right) \quad (64)$$

$$\sin \sqrt{2} \tilde{\phi}_s = -\cos \sqrt{2} \tilde{\theta}_s \quad (65)$$

$$\cos \sqrt{2} \tilde{\phi}_s = \cos \left(\sqrt{2} \tilde{\phi}_s + \frac{h_s x}{u_s} \right). \quad (66)$$

Since for the rung current in the mean-field approximation we have:

$$J_\perp(j) = \frac{\Omega}{\pi a} \left(2A_0^2 \sin\left(\frac{\lambda x}{a} - \sqrt{2}\tilde{\theta}_s\right) - 2A_0A_1 \sin(\sqrt{2}\tilde{\theta}_s) \cos(\sqrt{2}\tilde{\phi}_s) - 2A_0A_1 \sin(\sqrt{2}\tilde{\theta}_s - 2\frac{\lambda x}{a}) \cos(\sqrt{2}\tilde{\phi}_s) \right) \quad (67)$$

after the rotation we find:

$$\begin{aligned} J_\perp(j) &= \frac{\Omega}{\pi a} \left[2A_0^2 \left(\sin\left(\frac{\lambda x}{a}\right) \sin\left(\sqrt{2}\tilde{\phi}_s + \frac{h_s x}{u_s}\right) - \cos\left(\frac{\lambda x}{a}\right) \sin(\sqrt{2}\tilde{\theta}_s) \right) \right. \\ &\quad - 2A_0A_1 \left(\sin(\sqrt{2}\tilde{\theta}_s + \frac{h_s x}{u_s})(1 + \cos(2\frac{\lambda x}{a})) \right) \\ &\quad \left. - 2A_0A_1 \sin(2\frac{\lambda x}{a}) \left(-\frac{1}{\pi \sqrt{2}} \partial_x \tilde{\phi}_s - \frac{h_s x}{u_s} \right) \right], \end{aligned} \quad (68)$$

so that:

$$\begin{aligned} \langle J_\perp(j) J_\perp(j') \rangle &\sim \frac{1}{(j-j')^2} \cos\left(\frac{h_s(j-j')}{u_s}\right) (1 + \cos 2\lambda j) (1 + \cos(2\lambda j')) + \\ &\quad \frac{1}{(j-j')^2} (1 + \sin(2\lambda j)) (1 + \sin(2\lambda j')) \\ &\quad + \sin(\lambda j) \sin(\lambda j') \cos\left(\frac{h_s(j-j')}{u_s}\right) \frac{1}{|j-j'|} + \cos(\lambda j) \cos(\lambda j') \frac{1}{|j-j'|}. \end{aligned} \quad (69)$$

We therefore see that an incommensuration develops in the $k \simeq 0$ and $k \sim 2\lambda = 2\pi\rho$ component of the rung-current and density-wave correlations. In the Fourier transform peaks are located at $\pi\rho$, $\pi\rho \pm h_s/u_s$ while the singularities at $2\pi\rho$ and $2\pi\rho \pm h_s/u_s$ are discontinuities of slope. Since $h_s \sim \Omega^2$, the incommensuration increases with interchain hopping. One can repeat the calculation also for the S_z operator and its correlation function $S_s(j-j') \sim \cos(\lambda j) \cos(\lambda j') \frac{1}{|j-j'|}$, giving rise to a peak at $k \sim \pm\pi\rho$.

Regarding the calculation of the momentum distribution, since the boson annihilation operators do not correspond to primary fields of the $SU(2)_1$ WZNW model, we cannot derive their expression in terms of $\tilde{\theta}_s$ and $\tilde{\phi}_s$ using the $SU(2)$ rotation. However, since $e^{i\theta_s}$ has conformal dimensions $(1/16, 1/16)$ its expression in terms of the fields $\tilde{\phi}_s$ and $\tilde{\theta}_s$ can be expressed as a sum of operators of conformal dimensions $(1/16, 1/16)$. A general expression for the case $\lambda = \pi$ has been derived previously⁸². The general form on n_k consisted of three peaks centered at $\pi\sigma \pm h_s/u_s$ and $\pi\sigma$ or a single broad peak $\pi\sigma$, depending on the value of Ω . In the present case, a broad peak centered at $2\lambda\sigma$ or a narrow peak at $2\lambda\sigma$ plus satellites centered at $2\lambda\sigma \pm h_s/u_s$ are expected. As we noted above, these results are valid provided we are at a commensurate filling and a charge gap is formed. At generic filling, or when

interactions in the charge sector are insufficiently repulsive, the $U(1)$ symmetry of the term (59) is reestablished by quantum fluctuations. The translational symmetry is then unbroken, and the fluctuations of ϕ_c increase the exponents.

In Fig. 3 we follow the appearance of the second incommensuration in the momentum distribution for the system at $\rho = 0.75$, spanning from below the critical $\lambda_c = \pi\rho = 0.75\pi$ up to $\lambda = \pi$, as from panels a) to f). At $\lambda = 0.75\pi$ the appearance of the secondary peaks are clearly detectable.

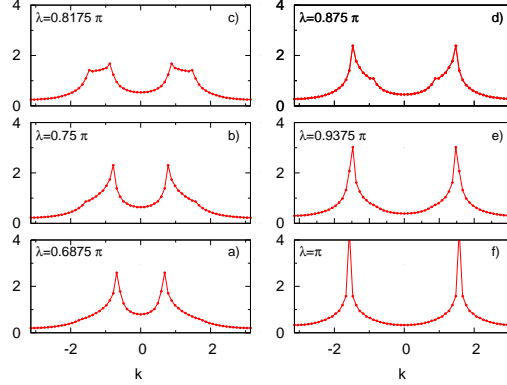


FIG. 3: Second incommensuration. DMRG simulation results at $L = 64$ in PBC. Momentum distribution $n(k)$ at $\rho = 0.75$ for different values of the applied flux λ as in the legend, spanning from below to well above the threshold $\lambda = 0.75$ for the appearance of the second incommensuration. The interchain hopping is fixed at the value $\Omega = 1.25$.

The positions of these peaks move towards zero with increasing the flux, and disappear completely at $\lambda = \pi$, where the system is back in the standard Vortex phase. In the presence of the second incommensuration, the position of the peaks is no more directly proportional to the applied flux: this is apparent in Fig. 4, where the position k_{max} of the peaks in the momentum distribution is displayed as a function of λ for the case with $\rho = 0.75$ and $\Omega = 1.25$ (red solid dots). For small values of Ω , the relation $q(\lambda) = \lambda$ is valid on a large range, and the possible deviation at critical λ is not appreciable, as it is seen in the Fig. 4 (open black dots).

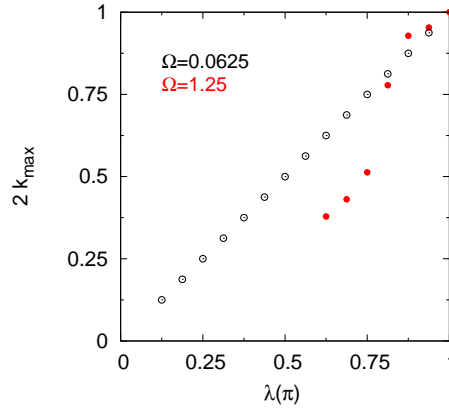


FIG. 4: Second incommensuration. DMRG simulation results at $L = 64$ in PBC. Position k_{max} of the peaks of the momentum distribution $n(k)$ at $\rho = 0.75$. Open black dots: $\Omega = 0.0625$. Red solid dots: $\Omega = 1.25$.

We can also follow the momentum distribution at the critical $\lambda_c = \pi\rho$ while varying the interchain hopping Ω . In Fig. 5 we show $n(k)$ for the system at $\rho = 0.5$ and fixed applied flux $\lambda = \pi/2$ on increasing the interchain hopping. For the case with $\Omega = 0.0625$, represented by the dashed black line, the gap in total density is too small to be detected in the present numerical simulation at the $L = 64$ system size. Yet, at $\Omega = 0.5$ and 0.75 the second incommensuration becomes clearly visible with the predicted appearance of the secondary peaks.

As mentioned above the effects of the gap opening manifest also in the correlation function for the rung-current.

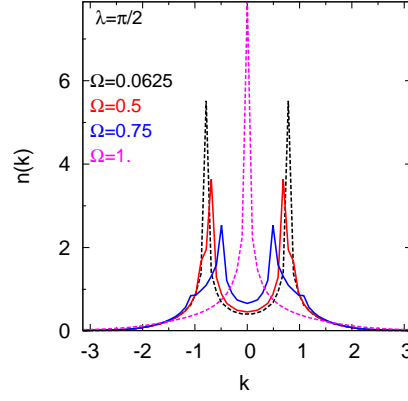


FIG. 5: Second incommensuration. DMRG simulation results at $L = 64$ in PBC. Momentum distribution $n(k)$ at $\rho = 0.5$ and fixed applied flux $\lambda = \pi\rho$, for different values of Ω as in the legend. Dashed black line: $\Omega = 0.0625$, where the system is in the standard vortex phase (first incommensuration). Dashed magenta line: $\Omega = 1$, where the system is in the Meissner phase. Red and blue solid lines: $\Omega = 0.5$ and $\Omega = 0.75$, respectively, where the occurrence of the second incommensuration is signaled by the appearance of the secondary peaks.

In Fig. 6 we show the FT of this quantity at $\lambda = 0.75\pi$ for different fillings. The left panel of Fig. 6 displays the data at a small value $\Omega = 0.0625$: here, the system is in the standard Vortex phase (first incommensuration) characterized by peaks located at $q(\lambda) = 0.75\pi$. For the $\rho = 0.75$ the small interchain hopping leads to a gap too small to be detected for the system size of the present simulation. In all filling cases the peaks are located at $k = q(\lambda) = 0.75\pi$ and $k = 2\pi - q(\lambda) = 5/4\pi$. The right panel of Fig. 6 displays the data at $\Omega = 0.75$, which is instead a sufficiently large value so that the second incommensuration becomes sizable: indeed, $C(k)$ gets the expected second structure at the predicted filling $\rho = 0.75$, while at smaller values of the filling no qualitative differences are seen with respect to the behavior shown in the left panel. At $\rho = 1.0$ the second incommensuration appears at $\lambda = \pi$ and the peak at $k = \pi$, and it is still detectable for this applied flux⁴¹.

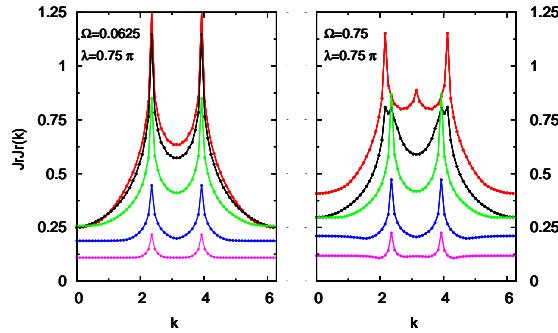


FIG. 6: First and second incommensuration. DMRG simulation results at $L = 64$ in PBC. FT of the rung-current correlation function $C(k)$ at fixed applied flux $\lambda = 0.75\pi$ for different fillings as in the legend: $\rho = 1.0, 0.75, 0.5, 0.25$ and 0.125 are represented by black, red, green, blue and magenta solid lines, respectively. Left panel: case with $\Omega = 0.0625$. Right panel: case with $\Omega = 0.75$. Data at $\Omega = 0.75$ and $\rho = 1$ as been shifted to make more evident the second incommensurations peaks.

As in the case $n = 1.0$ ⁴¹ indeed, there is a large region of stability of the second incommensuration near the critical value of λ . In order to show the typical behavior, we summarize in Fig. 7 the phase diagram at the selected filling $\rho = 0.5$, which evidences the boundary in the transition from Meissner to Vortex phase and the extension of the region where is possible to detect the second incommensuration, as resulting from DMRG simulations in PBC for a system size $L = 64$.

In Fig. 8 we show the behavior of $S_s(k)$ for different fillings in two different situations in which only the first or

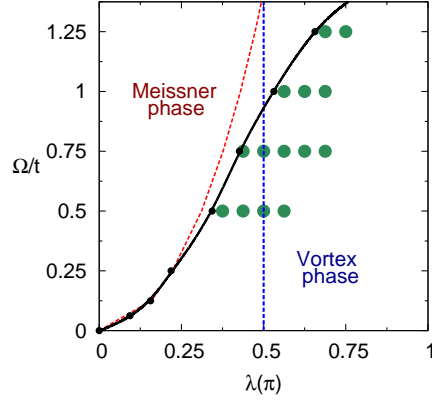


FIG. 7: DMRG simulation results at $L = 64$ in PBC. Phase diagram for a hard-core bosonic system on ladder as a function of flux per plaquette λ and Ω , at the filling value $\rho = 0.5$. The occurrence of the two incommensurations is evidenced as follows. The black solid line represents the phase boundary between the Meissner and the first incommensuration, a standard Vortex phase. The dark-green solid dots are the points where the second incommensuration appears. The dashed blue line marks the critical $\lambda = 0.5\pi$ at which the second incommensuration is expected. For comparison, the phase boundary between the Meissner and Vortex phase for a non-interacting system is represented as well, by the red-dashed line. Notice the enhanced size⁴⁰ of the Meissner region in the hard-core repulsive with respect to the non-interacting case.

also the second incommensuration appear. In the left panel, the behavior in the standard vortex phase is displayed, after picking small values of λ and Ω . In the right panel, we show the behavior at $\lambda = 0.25\pi$: here, the appearance of the second incommensuration is expected at $\rho = 0.25$, characterized by two peaks develop at $k = 0.25\pi$ and $k = 2\pi - 0.25\pi$, and with $S_s(k \rightarrow 0)$ getting a sizable finite value and a linear momentum dependence. At the other fillings, the spin correlation function gets small finite values at $k = 0$ and very low peaks at $k = \rho\pi$ and $k = 2\pi - \rho\pi$, apart from the case $\rho = 0.125$ already in the Meissner phase.

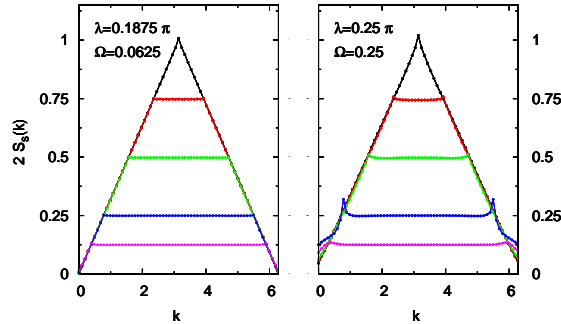


FIG. 8: DMRG simulation results at $L = 64$ in PBC. Spin static structure factor $S_s(k)$ for different fillings as in the legend: $\rho = 1.0, 0.75, 0.5, 0.25,$ and 0.125 are represented by the black, red, green, blue, and magenta solid lines, respectively. Left panel: $\lambda = 0.1875\pi$ and the small value of interchain hopping $\Omega = 0.0625$, where the system is always in the standard Vortex phase at all fillings. Right panel: $\lambda = 0.25\pi$ and $\Omega = 0.25$. Notice that the system at $\rho = 0.125$ is in the Meissner phase.

We conclude this section summarizing in Fig. 9 the effects that the appearance of the second incommensuration produces in the different observables and quantities analyzed in the text. We see that there is almost no effect on the charge static structure factor $S_c(k)$: as shown in Fig. 1 or Fig. 2, in fact no sharp slope discontinuity at $k = \rho\pi$ and $k = 2\pi - \rho\pi$ emerges in the second incommensuration with respect to the first, that is the standard vortex case. We remark the difference between the $\rho < 1$ cases here mainly analyzed and the $\rho = 1.0$ case, which instead corresponds to a Mott-insulator, *i.e.* quadratic behavior at low momenta. On the other hand, DMRG data show a gap closure for $\rho < 1$: in fact, the Mermin-Wagner theorem^{75,76} implies no breaking of the $U(1)$ symmetry $\phi_c \rightarrow \phi_c + \alpha$,

$\theta_s \rightarrow \theta_s - \alpha$, so that we conjecture that fluctuations beyond mean field close the charge gap, but do not eliminate the incommensuration.

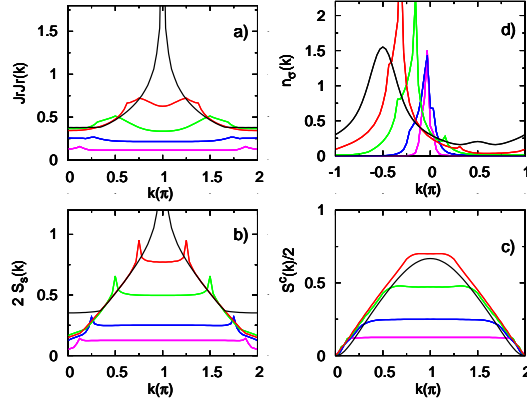


FIG. 9: DMRG simulation results at $L = 64$ in PBC. Summary of the FT observables behavior at different fillings: $\rho = 1.0, 0.75, 0.5, 0.25,$ and 0.125 are represented by the black, red, green, blue, and magenta solid lines, respectively. The value of λ is set to $\lambda = \pi\rho$ and Ω is chosen in order to make the second incommensuration visible. Panel a): rung-current correlation function $C(k)$. Panel b): spin correlation function $S_s(k)$. Panel c): twice the charge correlation function $2S_c(k)$. Panel d): (spin-) chain-resolved momentum distribution $n_\sigma(k)$, with $n_{-\sigma}(k) = n_\sigma(k)$. The different curve color represent different values of Ω as follows: $\Omega = 1.25$ (black), $\Omega = 1$ (red), $\Omega = 0.75$ (green), $\Omega = 0.25$ (blue), and $\Omega = 0.0625$ (magenta).

IV. CONCLUSION

In conclusion, we have analyzed the appearance and evolution of a second incommensuration in the phase diagram of a boson two-leg ladder with equal densities in each chain at varying the system parameters as the interchain hopping, the flux per plaquette, and the filling. A comparison between the predictions of the bosonization treatment and the results of DMRG simulations on the commensurate-incommensurate transition from a commensurate Meissner to a standard incommensurate Vortex phase, and the second incommensuration, has been discussed. As predicted by bosonization⁴¹, the occurrence of a second incommensuration has been found whenever the ratio between the flux and the filling is equal to π , and confirmed indeed by the DMRG simulations. The developing of the second incommensuration can be followed in the momentum distribution, that can be readily measured in experiments³¹. Our DMRG results have been summarized in the interchain hopping-flux phase diagram Fig. 7 at half-filling, displaying the extensions of the Meissner phase, as well as the occurrence of the first incommensuration (standard Vortex phase) and second incommensuration. The trace of the second incommensuration on observables and correlation functions has been summed up in Fig. 9.

A few questions remain open for future investigations. For example, one could investigate whether a second incommensuration would also be observed in multi-chain systems, such as a ladder with a few legs or a two-dimensional array of bosonic chains.

Our predictions can be tested in current experiments, where observables that we have analyzed and discussed can be accessed. We remark that this system appears to show a significant sensitivity while evolving from the commensurate Meissner to each of the two incommensurate phases, which can be an interesting property to be exploited in possible applications.

Appendix A: Mapping to a spin ladder

In the hard core boson case, a representation⁸³ in terms of (pseudo) spins 1/2 can be introduced:

$$b_{j,\uparrow}^\dagger = S_{j,1}^+ b_{j,\downarrow}^\dagger = S_{j,2}^+, \quad (\text{A1})$$

$$b_{j,\uparrow} = S_{j,1}^- b_{j,\downarrow} = S_{j,2}^-, \quad (\text{A2})$$

$$b_{j,\uparrow}^\dagger b_{j,\uparrow} = S_{j,1}^z + \frac{1}{2} b_{j,\downarrow}^\dagger b_{j,\downarrow} = S_{j,2}^z + \frac{1}{2}, \quad (\text{A3})$$

With such mapping, we can rewrite the Hamiltonian (1) as a two-leg ladder Hamiltonian:

$$H = \sum_{r=1,2}^j J(S_{j,r}^x S_{j+1,r}^x + S_{j,r}^y S_{j+1,r}^y) + (-1)^r D(S_{j,r}^y S_{j+1,r}^x - S_{j,r}^x S_{j+1,r}^y) \quad (\text{A4})$$

$$+ \sum_j J_{\perp}(S_{j,1}^+ S_{j,2}^- + S_{j,1}^- S_{j,2}^+) + J_{\perp}^z S_{j,1}^z S_{j,2}^z \quad (\text{A5})$$

$$- \mu \sum_j (S_{j,1}^z + S_{j,2}^z) + h \sum_j (S_{j,1}^z - S_{j,2}^z), \quad (\text{A6})$$

where $J = t \cos \lambda$, $D = t \sin \lambda$, $J_{\perp} = \frac{\Omega}{2}$, $J_{\perp}^z = U_{\uparrow\downarrow}$ and $h = \delta/2$. The term D is a uniform Dzyaloshinskii-Moriya (DM)^{42,43,84,85} interaction, with the DM vector parallel to z . For $\delta \neq 0$, the two legs of the ladder are exposed to a different magnetic field.

Appendix B: Fermionization and single-particle correlation functions

The fermionized Hamiltonian (44) is obtained by the following correspondence with the boson operators:

$$\psi_R^{\dagger} \psi_R + \psi_L^{\dagger} \psi_L = -\frac{\partial_x \theta_s}{\pi \sqrt{2}} \quad (\text{B1})$$

$$\psi_R^{\dagger} \psi_R - \psi_L^{\dagger} \psi_L = \frac{\sqrt{2} \partial_x \phi_s}{\pi} \quad (\text{B2})$$

$$\psi_R^{\dagger} \psi_L + \psi_L^{\dagger} \psi_R = \frac{\cos \sqrt{2} \theta_s}{\pi \alpha} \quad (\text{B3})$$

$$-i(\psi_R^{\dagger} \psi_L - \psi_L^{\dagger} \psi_R) = \frac{\sin \sqrt{2} \theta_s}{\pi \alpha} \quad (\text{B4})$$

Within fermionization approach the single-particle correlation function $\langle \psi_R^{\dagger} \psi_L \rangle$ can be evaluated by the single-particle Green's function of the operators that diagonalize the Hamiltonian (46)

$$\langle \psi_R^{\dagger} \psi_L \rangle = \int \frac{dk}{2\pi} \sin \varphi_k \cos \varphi_k \langle c_{k,+}^{\dagger} c_{k,+} - c_{k,-}^{\dagger} c_{k,-} \rangle \quad (\text{B5})$$

$$= \int_{\sqrt{h^2 - \Delta^2}/u}^{\Lambda} \frac{dk}{2\pi} \frac{m}{\sqrt{uk^2 + m^2}} \quad (\text{B6})$$

$$= \frac{m}{4\pi v} \ln \left(\frac{2v\Lambda}{h + \sqrt{h^2 - m^2}} \right). \quad (\text{B7})$$

since $\langle \psi_R^{\dagger} \psi_L \rangle$ is real, there is no average current between the legs of the ladder. However, it is possible to find fluctuations of the current as shown in Eq.51. In the commensurate phase the correlators can be evaluated using (46) and one obtains

$$\langle \psi_R^{\dagger}(x) \psi_L(x') \rangle = - \int_{-\infty}^{\infty} \frac{dk}{4\pi} \frac{m}{\sqrt{(uk)^2 + m^2}} e^{ik(x'-x)}, \quad (\text{B8})$$

$$\langle \psi_L^{\dagger}(x) \psi_R(x') \rangle = - \int_{-\infty}^{\infty} \frac{dk}{4\pi} \frac{m}{\sqrt{(uk)^2 + m^2}} e^{ik(x'-x)}, \quad (\text{B9})$$

$$\langle \psi_R^{\dagger}(x) \psi_R(x') \rangle = - \int_{-\infty}^{\infty} \frac{dk}{4\pi} \frac{uk}{\sqrt{(uk)^2 + m^2}} e^{ik(x'-x)}, \quad (\text{B10})$$

$$\langle \psi_L^{\dagger}(x) \psi_L(x') \rangle = \int_{-\infty}^{\infty} \frac{dk}{4\pi} \frac{uk}{\sqrt{(uk)^2 + m^2}} e^{ik(x'-x)}, \quad (\text{B11})$$

so that:

$$\langle \psi_R^\dagger(x) \psi_L(x') \rangle = \langle \psi_L^\dagger(x) \psi_R(x') \rangle = -\frac{m}{2\pi u} K_0 \left(\frac{m|x-x'|}{u} \right), \quad (\text{B12})$$

$$\langle \psi_R^\dagger(x) \psi_R(x') \rangle = -\langle \psi_L^\dagger(x) \psi_L(x') \rangle = i \text{sign}(x-x') \frac{m}{2\pi u} K_1 \left(\frac{m|x-x'|}{u} \right), \quad (\text{B13})$$

where K_0 and K_1 are modified Bessel functions. This leads to the result (53) and one expects an exponential decay of the rung current correlation with correlation length $u/(2m)$.

In the incommensurate phase, the fermion correlation functions are expressible instead in terms of incomplete Bessel functions⁷³:

$$\epsilon_\nu(w, z) = \frac{1}{i\pi} \int_0^w e^{z \sinh t - \nu t} dt \quad (\text{B14})$$

Indeed, we have (for $T = 0$):

$$\langle \psi_R^\dagger(x) \psi_L(x') \rangle = \int_{-k_F}^{k_F} \frac{dk}{4\pi} \frac{m}{\sqrt{(uk)^2 + m^2}} e^{ik(x'-x)} - \int_{-\infty}^{\infty} \frac{dk}{4\pi} \frac{m}{\sqrt{(uk)^2 + m^2}} e^{ik(x'-x)}, \quad (\text{B15})$$

$$\langle \psi_R^\dagger(x) \psi_R(x') \rangle = \int_{-k_F}^{k_F} \frac{dk}{4\pi} \left(1 + \frac{uk}{\sqrt{(uk)^2 + m^2}} \right) e^{ik(x'-x)} - \int_{-\infty}^{\infty} \frac{dk}{4\pi} \frac{uk}{\sqrt{(uk)^2 + m^2}} e^{ik(x'-x)}, \quad (\text{B16})$$

$$\langle \psi_L^\dagger(x) \psi_L(x') \rangle = \int_{-k_F}^{k_F} \frac{dk}{4\pi} \left(1 - \frac{uk}{\sqrt{(uk)^2 + m^2}} \right) e^{ik(x'-x)} + \int_{-\infty}^{\infty} \frac{dk}{4\pi} \frac{uk}{\sqrt{(uk)^2 + m^2}} e^{ik(x'-x)}, \quad (\text{B17})$$

where $\sqrt{(uk_F)^2 + m^2} = h$ and we have noted that $\langle \psi_R^\dagger(x) \psi_L(x') \rangle = \langle \psi_L^\dagger(x) \psi_R(x') \rangle$. In Eq.(B15), we have two contributions, one coming from the partially filled upper band, and the other from the filled lower band which was the only contribution in the commensurate case. We see that when $h \rightarrow +\infty$, $k_F \rightarrow \infty$ and $\langle \psi_R^\dagger(x) \psi_L(x') \rangle \rightarrow 0$ uniformly. We have:

$$\begin{aligned} \int_{-k_F}^{k_F} \frac{dk}{4\pi} \frac{m}{\sqrt{(uk)^2 + m^2}} e^{ik(x'-x)} &= \frac{m}{u} \int_{-\theta_F}^{\theta_F} \frac{d\theta}{4\pi} e^{i \frac{m(x'-x)}{u} \sinh \theta} \\ &= \frac{im}{4u} \left[\epsilon_0 \left(\theta_F, i \frac{m(x'-x)}{u} \right) - \epsilon_0 \left(-\theta_F, i \frac{m(x'-x)}{u} \right) \right] \end{aligned} \quad (\text{B18})$$

$$\begin{aligned} \int_{-k_F}^{k_F} \frac{dk}{4\pi} \frac{uk}{\sqrt{(uk)^2 + m^2}} e^{ik(x'-x)} &= \frac{m}{u} \int_{-\theta_F}^{\theta_F} \frac{d\theta}{4\pi} e^{i \frac{m(x'-x)}{u} \sinh \theta} \sinh \theta \\ &= \frac{im}{8u} \left[\epsilon_1 \left(\theta_F, i \frac{m(x'-x)}{u} \right) - \epsilon_{-1} \left(\theta_F, i \frac{m(x'-x)}{u} \right) - \epsilon_1 \left(-\theta_F, i \frac{m(x'-x)}{u} \right) \right. \\ &\quad \left. + \epsilon_{-1} \left(-\theta_F, i \frac{m(x'-x)}{u} \right) \right] \end{aligned} \quad (\text{B19})$$

and thus:

$$\langle \psi_R^\dagger(x) \psi_L(x') \rangle = \frac{im}{4u} \left[\epsilon_0 \left(\theta_F, i \frac{m(x'-x)}{u} \right) - \epsilon_0 \left(-\theta_F, i \frac{m(x'-x)}{u} \right) \right] - \frac{m}{2\pi u} K_0 \left(\frac{m|x-x'|}{u} \right) \quad (\text{B20})$$

$$\begin{aligned} \langle \psi_R^\dagger(x) \psi_R(x') \rangle &= \frac{\sin k_F(x'-x)}{2\pi(x'-x)} + \frac{im}{8u} \left[\epsilon_1 \left(\theta_F, i \frac{m(x'-x)}{u} \right) - \epsilon_{-1} \left(\theta_F, i \frac{m(x'-x)}{u} \right) - \epsilon_1 \left(-\theta_F, i \frac{m(x'-x)}{u} \right) \right. \\ &\quad \left. + \epsilon_{-1} \left(-\theta_F, i \frac{m(x'-x)}{u} \right) \right] + i \text{sign}(x-x') \frac{m}{2\pi u} K_1 \left(\frac{m|x-x'|}{u} \right) \\ \langle \psi_L^\dagger(x) \psi_L(x') \rangle &= \frac{\sin k_F(x'-x)}{2\pi(x'-x)} - \frac{im}{8u} \left[\epsilon_1 \left(\theta_F, i \frac{m(x'-x)}{u} \right) - \epsilon_{-1} \left(\theta_F, i \frac{m(x'-x)}{u} \right) - \epsilon_1 \left(-\theta_F, i \frac{m(x'-x)}{u} \right) \right. \\ &\quad \left. + \epsilon_{-1} \left(-\theta_F, i \frac{m(x'-x)}{u} \right) \right] - i \text{sign}(x-x') \frac{m}{2\pi u} K_1 \left(\frac{m|x-x'|}{u} \right) \end{aligned} \quad (\text{B21})$$

For large distances, $|x-x'| \gg u/m$, we can neglect the contribution from the lower band. The contribution from the upper band can be obtained from the asymptotic expansions given in Ref. 73 on p. 146, while the simpler derivation can be obtained from physical arguments and is presented in the main text. Indeed, in the case $uk_F \ll m$, we can make the approximations:

$$\frac{m}{\sqrt{(uk)^2 + m^2}} \simeq 1 \quad (\text{B22})$$

$$\frac{uk}{\sqrt{(uk)^2 + m^2}} \simeq \frac{uk}{m} \quad (\text{B23})$$

giving:

$$\langle \psi_R^\dagger(x) \psi_L(x') \rangle \simeq \frac{\sin k_F(x' - x)}{2\pi(x' - x)} + O(x - x')^{-3} \quad (\text{B24})$$

$$\langle \psi_R^\dagger(x) \psi_R(x') \rangle = \frac{\sin k_F(x' - x)}{2\pi(x' - x)} - \frac{iuk_F}{m} \left[\frac{\cos k_F(x' - x)}{2\pi(x' - x)} + \frac{\sin k_F(x' - x)}{2\pi k_F(x' - x)^2} \right] + O(x - x')^{-3} \quad (\text{B25})$$

$$\langle \psi_L^\dagger(x) \psi_L(x') \rangle = \frac{\sin k_F(x' - x)}{2\pi(x' - x)} + \frac{iuk_F}{m} \left[\frac{\cos k_F(x' - x)}{2\pi(x' - x)} + \frac{\sin k_F(x' - x)}{2\pi k_F(x' - x)^2} \right] + O(x - x')^{-3} \quad (\text{B26})$$

Second, in the case of $uk_F \gg m$, we can linearize the dispersion in the upper band around the points $\pm k_F$. We can then make the approximations:

$$\frac{u(k \pm k_F)}{\sqrt{u^2(k \pm k_F)^2 + m^2}} \simeq \pm 1 \quad (\text{B27})$$

This time, we find:

$$\langle \psi_R^\dagger(x) \psi_R(x') \rangle = e^{ik_F(x' - x)} \int_{-\infty}^0 \frac{dk}{2\pi} e^{k(\alpha + i(x' - x))} = \frac{e^{ik_F(x' - x)}}{2\pi(\alpha + i(x' - x))} \quad (\text{B28})$$

$$\langle \psi_L^\dagger(x) \psi_L(x') \rangle = e^{-ik_F(x' - x)} \int_0^{+\infty} \frac{dk}{2\pi} e^{k(-\alpha + i(x' - x))} = \frac{e^{-ik_F(x' - x)}}{2\pi(\alpha - i(x' - x))} \quad (\text{B29})$$

$$\langle \psi_R^\dagger(x) \psi_L(x') \rangle = \frac{m}{2\pi uk_F} \frac{\sin k_F(x' - x)}{(x' - x)} \quad (\text{B30})$$

We see that the correlator $\langle \psi_R^\dagger(x) \psi_L(x') \rangle$ is smaller by a factor $m/(uk_F) \sim m/h \ll 1$ in that limit. If we had instead written a bosonized Hamiltonian, we would have found that $\langle \psi_R^\dagger(x) \psi_L(x') \rangle = 0$. With Eqs.(B28), we obtain the expression for the rung-current correlator (56).

-
- ¹ M. Tinkham, *Introduction to Superconductivity* (McGraw Hill, New York, 1975).
² M. Kardar, Phys. Rev. B **33**, 3125 (1986).
³ E. Orignac and T. Giamarchi, Phys. Rev. B **64**, 144515 (2001), cond-mat/0011497.
⁴ M.-C. Cha and J.-G. Shin, Phys. Rev. A **83**, 055602 (2011).
⁵ G. I. Japaridze and A. A. Nersesyan, JETP Lett. **27**, 334 (1978).
⁶ V. L. Pokrovsky and A. L. Talapov, Phys. Rev. Lett. **42**, 65 (1979).
⁷ H. J. Schulz, Phys. Rev. B **22**, 5274 (1980).
⁸ E. Granato, Phys. Rev. B **42**, 4797 (1990).
⁹ Y. Nishiyama, Eur. Phys. J. B **17**, 295 (2000), cond-mat/0006311.
¹⁰ A. Dhar, M. Maji, T. Mishra, R. V. Pai, S. Mukerjee, and A. Paramekanti, Phys. Rev. A **85**, 041602 (2012).
¹¹ A. Dhar, T. Mishra, M. Maji, R. V. Pai, S. Mukerjee, and A. Paramekanti, Phys. Rev. B **87**, 174501 (2013).
¹² A. Petrescu and K. Le Hur, Phys. Rev. Lett. **111**, 150601 (2013).
¹³ A. Petrescu and K. Le Hur, Phys. Rev. B **91**, 054520 (2015).
¹⁴ A. van Oudenaarden and J. E. Mooij, Phys. Rev. Lett. **76**, 4947 (1996).
¹⁵ A. van Oudenaarden, S. J. K. Várdu, and J. Mooij, Phys. Rev. Lett. **77**, 4257 (1996).
¹⁶ R. Fazio and H. van der Zant, Phys. Rep. **355**, 235 (2001).
¹⁷ K. Le Hur, L. Henriot, A. Petrescu, K. Plekhanov, G. Roux, and M. Schiró, *Many-body quantum electrodynamics networks: Non-equilibrium condensed matter physics with light*, arXiv:1505.00167 (2015).

- ¹⁸ R. M. Bradley and S. Doniach, Phys. Rev. B **30**, 1138 (1984).
- ¹⁹ L. I. Glazman and A. I. Larkin, Phys. Rev. Lett. **79**, 3736 (1997).
- ²⁰ S. E. Korshunov, Europhys. Lett. **9**, 107 (1989).
- ²¹ P. A. Bobbert, R. Fazio, G. Schön, and G. T. Zimanyi, Phys. Rev. B **41**, 4009 (1990).
- ²² P. A. Bobbert, R. Fazio, G. Schön, and A. D. Zaikin, Phys. Rev. B **45**, 2294 (1992).
- ²³ C. Bruder, L. I. Glazman, A. I. Larkin, J. E. Mooij, and A. van Oudenaarden, Phys. Rev. B **59**, 1383 (1999).
- ²⁴ D. Jaksch and P. Zoller, Ann. Phys. (N. Y.) **315**, 52 (2005).
- ²⁵ M. Lewenstein, A. Sanpera, V. Ahufinger, B. Damski, A. Sen De, and U. Sen, Ann. Phys. (N. Y.) **56**, 243 (2007).
- ²⁶ I. Bloch, J. Dalibard, and W. Zwerger, Rev. Mod. Phys. **80**, 885 (2008).
- ²⁷ K. Osterloh, M. Baig, L. Santos, P. Zoller, and M. Lewenstein, Phys. Rev. Lett. **95**, 010403 (2005).
- ²⁸ J. Ruseckas, G. Juzeliūnas, P. Öhberg, and M. Fleischhauer, Phys. Rev. Lett. **95**, 010404 (2005).
- ²⁹ Y. Lin, K. Jimenez-Garcia, and I. B. Spielman, Nature **471**, 83 (2011).
- ³⁰ V. Galitski and I. B. Spielman, Nature (London) **494**, 49 (2013).
- ³¹ M. Atala, M. Aidelsburger, M. Lohse, J. Barreiro, B. Paredes, and I. Bloch, Nature Physics **10**, 588 (2014).
- ³² A. Tokuno and A. Georges, New J. Phys. **16**, 073005 (2014).
- ³³ J. Zhao, S. Hu, J. Chang, F. Zheng, P. Zhang, and X. Wang, Phys. Rev. B **90**, 085117 (2014).
- ³⁴ A. Keleş and M. O. Oktel, Phys. Rev. A **91**, 013629 (2015).
- ³⁵ Z. Xu, W. Cole, and S. Zhang, Phys. Rev. A **89**, 051604(R) (2014).
- ³⁶ M. Piraud, Z. Cai, I. P. McCulloch, and U. Schollwöck, Phys. Rev. A **89**, 063618 (2014).
- ³⁷ L. Barbiero, M. Abad, and A. Recati, *Magnetic phase transition in coherently coupled bose gases in optical lattices*, arXiv:1403.4185 (2014).
- ³⁸ S. Peotta, L. Mazza, E. Vicari, M. Polini, R. Fazio, and D. Rossini, J. Stat. Mech.: Theor. Exp. **2014**, P09005 (2014).
- ³⁹ A. Sterdyniak, M. Dalmonte, S. Manmana, P. Zoller, et al., Bulletin of the American Physical Society **59**(1) (2014), abstract: Z35.00007, URL <http://meetings.aps.org/link/BAPS.2014.MAR.Z35.7>.
- ⁴⁰ M. Piraud, F. Heidrich-Meisner, I. P. McCulloch, S. Greschner, T. Vekua, and U. Schollwöck, Phys. Rev. B **91**, 140406 (2015).
- ⁴¹ M. Di Dio, S. De Palo, E. Orignac, R. Citro, and M.-L. Chiofalo, Phys. Rev. B **92**, 060506 (2015).
- ⁴² I. Dzyaloshinskii, J. Phys. Chem. Solids **4**, 241 (1958).
- ⁴³ T. Moriya, Phys. Rev. **120**, 91 (1960).
- ⁴⁴ F. Crépin, N. Laflorencie, G. Roux, and P. Simon, Phys. Rev. B **84**, 054517 (2011).
- ⁴⁵ F. D. M. Haldane, Phys. Rev. Lett. **47**, 1840 (1981).
- ⁴⁶ A. A. Ovchinnikov, Journal of Physics Condensed Matter **16**, 3147 (2004).
- ⁴⁷ S. Coleman, Phys. Rev. D **11**, 2088 (1975).
- ⁴⁸ A. Luther, Phys. Rev. B **15**, 403 (1977).
- ⁴⁹ R. Rajaraman, *Solitons and Instantons: An Introduction to solitons and Instantons in Quantum Field Theory* (North Holland, Amsterdam, 1982).
- ⁵⁰ A. B. Zamolodchikov and A. B. Zamolodchikov, Ann. Phys. (N. Y.) **120**, 253 (1979).
- ⁵¹ P. Dorey, *Exact s-matrices* (1998), hep-th/9810026.
- ⁵² A. B. Zamolodchikov, Int. J. Mod. Phys. A **10**, 1125 (1995).
- ⁵³ M. A. Cazalilla, R. Citro, T. Giamarchi, E. Orignac, and M. Rigol, Rev. Mod. Phys. **83**, 1405 (2011).
- ⁵⁴ M. Oshikawa and I. Affleck, Phys. Rev. Lett. **79**, 2883 (1997).
- ⁵⁵ I. Affleck and M. Oshikawa, Phys. Rev. B **60**, 1039 (1999), Phys. Rev. B **62**, 9200(E) (2000).
- ⁵⁶ F. H. L. Essler, Phys. Rev. B **59**, 14376 (1999).
- ⁵⁷ F. H. L. Essler, A. Furusaki, and T. Hikihara, Phys. Rev. B **68**, 64410 (2003).
- ⁵⁸ H. Nojiri, Y. Ajiro, T. Asano, and J.-P. Boucher, New J. Phys. **8**, 218 (2006).
- ⁵⁹ I. Umegaki, H. Tanaka, T. Ono, M. Oshikawa, and K. Sakai, Phys. Rev. B **85**, 144423 (2012).
- ⁶⁰ S. Lukyanov and A. B. Zamolodchikov, Nucl. Phys. B **493**, 571 (1997).
- ⁶¹ G. S. Uhrig and H. J. Schulz, Phys. Rev. B **54**, R9624 (1996).
- ⁶² I. Affleck, Nucl. Phys. B **265**, 448 (1986).
- ⁶³ A. M. Tsvelik, Phys. Rev. B **45**, 486 (1992).
- ⁶⁴ H. G. Vaidya and C. A. Tracy, Phys. Rev. Lett. **42**, 3 (1979), *ibid.* **43**, 1540 (1979).
- ⁶⁵ D. M. Gangardt, J. Phys. A **37**, 9335 (2004).
- ⁶⁶ A. Luther and V. J. Emery, Phys. Rev. Lett. **33**, 589 (1974).
- ⁶⁷ E. Papa and A. M. Tsvelik, Phys. Rev. B **61**, 085109 (2001).
- ⁶⁸ R. Chitra and T. Giamarchi, Phys. Rev. B **55**, 5816 (1997).
- ⁶⁹ S. R. White, Phys. Rev. B **48**, 10345 (1993).
- ⁷⁰ U. Schollwöck, Rev. Mod. Phys. **77**, 259 (2005).
- ⁷¹ M. Di Dio, R. Citro, S. De Palo, E. Orignac, and M.-L. Chiofalo, Eur. Phys. J. Spec. Top. **224**, 525 (2015).
- ⁷² M. Abramowitz and I. Stegun, eds., *Handbook of mathematical functions* (Dover, New York, 1972).
- ⁷³ M. M. Agrest and M. Z. Maksimov, *Theory of incomplete cylindrical functions and their applications*, vol. 160 of *Grundlehren der mathematischen Wissenschaften* (Springer, Heidelberg, 1971).
- ⁷⁴ A. O. Gogolin, A. A. Nersisyan, and A. M. Tsvelik, *Bosonization and Strongly Correlated Systems* (Cambridge University Press, Cambridge, 1999).

- ⁷⁵ N. D. Mermin and H. Wagner, Phys. Rev. Lett. **17**, 1133 (1967).
- ⁷⁶ P. C. Hohenberg, Phys. Rev. **158**, 383 (1967).
- ⁷⁷ A. A. Nersesyan, A. O. Gogolin, and F. H. L. Essler, Phys. Rev. Lett. **81**, 910 (1998).
- ⁷⁸ P. Lecheminant, T. Jolicoeur, and P. Azaria, Phys. Rev. B **63**, 174426 (2001).
- ⁷⁹ T. Jolicoeur and P. Lecheminant, Prog. Theor. Phys. Supp. **145**, 23 (2002).
- ⁸⁰ M. Zarea, M. Fabrizio, and A. Nersesyan, Eur. Phys. J. B **39**, 155 (2004).
- ⁸¹ A. Nersesyan, A. Luther, and F. Kusmartsev, Phys. Lett. A **176**, 363 (1993).
- ⁸² M. Di Dio, S. De Palo, E. Orignac, R. Citro, and M.-L. Chiofalo, *Supplemental material for "persisting meissner state and incommensurate phases of hard-core boson ladders in a flux"*, <http://link.aps.org/supplemental/10.1103/PhysRevB.92.060506> (2015).
- ⁸³ M. E. Fisher, Rep. Prog. Phys. **30**, 615 (1967), and references therein.
- ⁸⁴ T. Kaplan, Z. Phys. B **49**, 313 (1983).
- ⁸⁵ L. Shekhtman, O. Entin-Wohlman, and A. Aharony, Phys. Rev. Lett. **69**, 836 (1992).